Experimental evidence for a valence-bond glass in the $5d^1$ double perovskite Ba_2YWO_6

S. Lee,[1] Wonjun Lee,[1] W. Guohua,[2] J. Ma,[2] H. Zhou,[3] M. Lee,[4] E. S. Choi,[4] and K.-Y. Choi[1,5,*]

[1]*Department of Physics, Chung-Ang University, 84 Heukseok-ro, Seoul 06974, Republic of Korea*

[2]*Key Laboratory of Artificial Structures and Quantum Control (Ministry of Education), Shenyang National Laboratory for Materials Science, School of Physics and Astronomy, Shanghai Jiao Tong University, Shanghai 200240, China*

[3]*Department of Physics and Astronomy, University of Tennessee, Knoxville, Tennessee 37996-1200, USA*

[4]*National High Magnetic Field Laboratory, Florida State University, Tallahassee, Florida 32310, USA*

[5]*Department of Physics, Sungkyunkwan University, Suwon 16419, Republic of Korea*

(Received 19 February 2021; revised 24 May 2021; accepted 7 June 2021; published 22 June 2021)

We report the magnetic susceptibility, specific heat, and muon spin relaxation results of the $5d^1$ double perovskite Ba_2YWO_6. The dc magnetic susceptibility shows two distinct Curie-Weiss regimes and a sub-Curie-Weiss increase T^{-n} with $n = 0.75(1)$ for $T = 3$–100 K, alluding to the presence of random magnetism. The ac magnetic susceptibility reveals a spin freezing at $T_f \sim 0.3$ K with the activation energy of $\Delta/k_B = 27.6$ K. The specific heat data exhibit the pseudogap behavior at 25 K and the subsequent power-law dependence with decreasing temperature, indicating the gradual spin freezing with the quenching of orbital fluctuations. However, the muon spin relaxation data display only a weak muon spin depolarization with lacking long-range magnetic ordering down to 26 mK. Taken together, our results suggest that Ba_2YWO_6 is the proximate realization of a random spin-orbit dimer state.

DOI: 10.1103/PhysRevB.103.224430

I. INTRODUCTION

A double perovskite (DP) $A_2BB'O_6$ family has gathered considerable attention due to its potential to host diverse exotic states of matter [1]. The magnetic phases can be controlled by the combination of magnetic or nonmagnetic cations on A, B, and B′ sites in DPs [2]. In general, the A site is occupied by nonmagnetic cations, while the B and B′ sites are possessed by transition-metal ions. The B and B′ ions form octahedra with surrounding oxygens, constituting two interpenetrating face-centered cubic (FCC) lattices [see Fig. 1(a)]. When magnetic ions reside in only one of the B or B′ sites, then a magnetic sublattice becomes a simple magnetic FCC lattice, which corresponds to an edge-sharing tetrahedral network [see Fig. 1(b)]. This structural motif underlies geometrical frustration in three dimensions.

In DPs with d^1 electronic configuration, a plethora of magnetic ground states and the unique interplay between spin and orbital and lattice have been predicted theoretically [3–5]. In the presence of strong spin-orbit coupling and Coulomb correlation, the $5d^1$ electron systems form a $j_{\rm eff} = 3/2$ Mott insulator. A conspicuous feature of the pure $j_{\rm eff} = 3/2$ state is a vanishing net magnetization due to the cancellation of the spin moment by the orbital moment. As such, pseudodipolar moments entailing charge quadrupoles and magnetic octupolar moments as well as strong spin-orbital entanglement provide key notions that underpin the physics of the $j_{\rm eff} = 3/2$ Mott insulator [3]. The cubic DPs made of the Os^{7+}, Re^{6+}, Mo^{5+}, and W^{5+} ions can realize such a $j_{\rm eff} = 3/2$ state. A range of experimentally reported magnetic ground states include a collective gapped singlet state in A_2YMoO_6 (A=Ba, Sr), a spin freezing in the absence of long-range order in $Ba_2Y_{2/3}ReO_6$, a ferromagnetic Mott-insulating state in Ba_2NaOsO_6 and Ba_2BReO_6 (B=Mg, Zn), and an antiferromagnetically ordered state in Ba_2LiOsO_6 [6–14].

One of the d^1 DPs, Ba_2YMoO_6 is known to have puzzling magnetic properties. The dc magnetic susceptibility and muon spin relaxation (μSR) results show no evidence of a magnetic transition down to 50 mK [7,8,10]. However, subsequent ac magnetic susceptibility measurements revealed the spin-freezing-like transition at 0.6 K [10]. The magnetic entropy reaches $R\ln 4$ at high T, suggesting the presence of an orbital degree of freedom along with the spin [7]. Based on these observations, a valence-bond glass state has been proposed, which is supported by the singlet-triplet excitation about 28 meV with in-gap magnetic states [9].

The valence-bond glass is characterized by an amorphous arrangement of dimers and the absence of magnetic ordering [15]. In contrast to a simple spin-singlet state, there is no electronic and magnetic gap but pseudogap is created by the additional orbital degree of freedom. Furthermore, the average spin value is zero on each lattice site as the spin rotational symmetry is preserved, as opposed to a spin glass state. The underlying mechanism of the valence-bond glass in the d^1 DPs lies in the fact that pseudospins $j_{\rm eff} = 3/2$ form spin-orbit dimers with inflated planar orbitals by spin-orbit coupling [4]. Remarkably, the spin-orbit dimer phase captures the experimental characteristics of the valence-bond glass state, including no long-range order or symmetry breaking

*choisky99@skku.edu

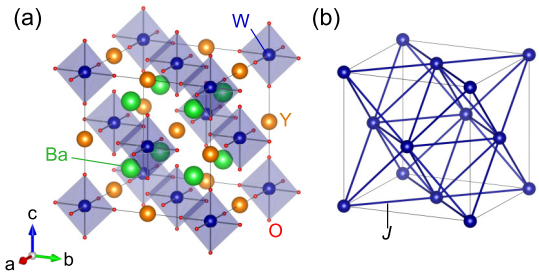

FIG. 1. (a) Crystal structure of Ba_2YWO_6. The W^{5+} ions are surrounded by six oxygens, forming WO_6 octahedra. The YO_6 octahedra are omitted for clarity. (b) The edge-sharing tetrahedral network consists of the coupled W spins via the super-superexchange interaction J (blue solid lines).

as well as pseudogap excitation allowed by magnetic dipole transition.

A related issue is on the relationship between quenched disorders and quantum-spin-liquid-like behaviors in frustrated magnets. There is accumulating theoretical and experimental evidence that disorders and exchange randomness often engender gapless quantum spin liquid-like states called a valence-bond glass or a random-singlet state [16]. The random singlets or valence-bond glass are characterized by a mixture of orphanlike spins and valence bonds (spin singlets) that own a broad distribution of their bond strength and number. In Ba_2YMoO_6, the valence-bond glass state remains stable against the isovalent substitution of Sr^{2+} for Ba^{2+} [17]. The ensuing question is whether the valence-bond glass is still retained in Ba_2YWO_6, which is the $5d^1$ counterpart of the $4d^1$ DP Ba_2YMoO_6.

In this paper, we present the dc and ac magnetic susceptibility, thermodynamic, and μSR measurements of Ba_2YWO_6. The dc and ac magnetic susceptibilities signal the development of a random magnetic state, which eventually undergoes a spin-freezing transition at $T_f \sim 0.3$ K. The specific heat data support the presence of significant orbital contributions to a total entropy and persistent orbital fluctuations. Furthermore, our μSR results exhibit a weak muon spin depolarization dictated by strongly quenched spin moments and the absence of long-range magnetic ordering down to 26 mK. These findings demonstrate that the valence-bond glass state observed in Ba_2YMoO_6 remains robust in Ba_2YWO_6 despite the variation of a spin-orbit strength and a stronger hybridization between W-5d and O-2p states.

II. EXPERIMENTAL DETAILS

Polycrystalline samples of Ba_2YWO_6 were synthesized by a solid-state reaction using a stoichiometric amount of the starting materials $BaCO_3$, WO_3, and Y_2O_3 (fine powder predried at 950°C overnight). The starting materials were mixed in agate mortars, pressed into pellets, and annealed in 10% H_2/90% Ar gas at 1300°C for 20 h. The quality of the samples was confirmed using x-ray diffraction measurements (space group $Fm\bar{3}m$ and $a = 8.3848$ Å), which are well consistent with Ref. [18].

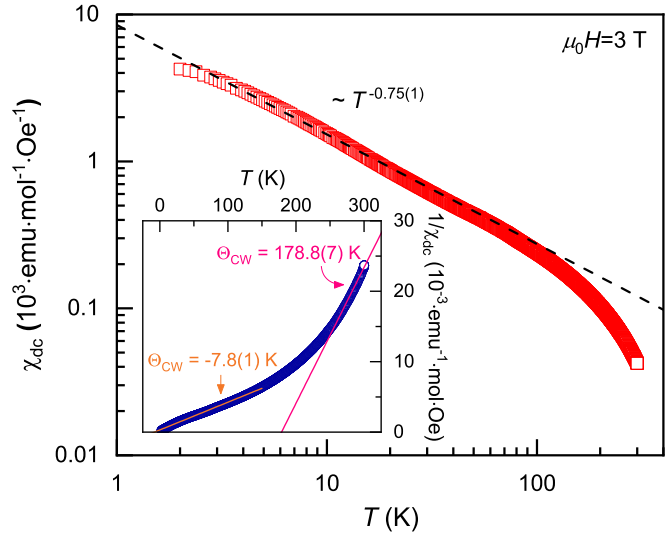

FIG. 2. Log-log plot of the dc magnetic susceptibility of Ba_2YWO_6 measured at 3 T. The black dashed line denotes the power-law behavior of $\chi_{dc}(T) \sim T^{-n}$ with $n = 0.75(1)$. The inset shows the inverse magnetic susceptibility $1/\chi_{dc}$ with the Curie-Weiss fits for two different temperature regions.

The dc magnetic susceptibility was measured using a SQUID (Quantum Design MPMS). The ac susceptibility was measured with the conventional mutual inductance technique with a homemade setup at the National High Magnetic Field Laboratory [19]. Specific heat was measured by the thermal-relaxation method in the PPMS with a ^{3}He insert, allowing for measurements down to 0.3 K.

μSR experiments were performed over the temperature range 26 mK $< T <$ 100 K on the πM3 beamline at the Paul Scherrer Institute (Villigen PSI, Switzerland) using the GPS spectrometer and on the M15 beamline at TRIUMF (Vancouver, Canada) using the dilution refrigerator. The polycrystalline samples Ba_2YWO_6 were ground and packaged with a silver foil and attached to the sample holder in PSI and TRIUMF. All obtained μSR data were analyzed using the software package MUSRFIT [20].

III. EXPERIMENTAL RESULTS

A. Magnetic susceptibility

Figure 2 exhibits the temperature dependence of the dc magnetic susceptibility $\chi_{dc}(T)$ of Ba_2YWO_6 on a log-log scale. An external magnetic field of 3 T is applied for our dc magnetic susceptibility measurements. With decreasing temperature, $\chi_{dc}(T)$ increases gradually and then shows a sub-Curie behavior below 100 K and, finally, tends to level off below 3 K.

We note that the inverse dc magnetic susceptibility $1/\chi_{dc}(T)$ shows two distinct Curie-Weiss regimes above 260 K and below 150 K, as displayed in the inset of Fig. 2. The Curie-Weiss analysis for high T yields $\Theta_{CW} = 178.8(7)$ K, $C = 0.00518(3)$ emu mol^{-1} K^{-1} Oe^{-1}, and $\mu_{eff} = 0.2035\ \mu_B$. The effective magnetic moment is much smaller than the expected value $\mu_{eff} = 1.73\ \mu_B$ for $S = 1/2$, being consistent with the suppressed spin moments for the

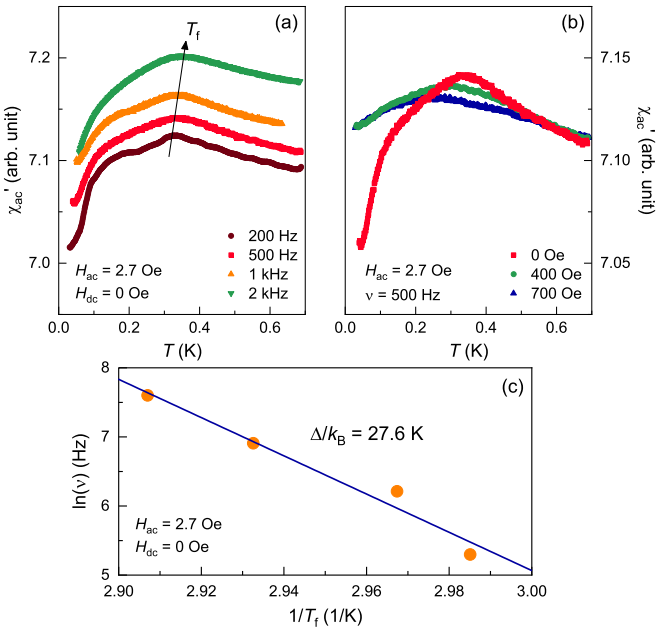

FIG. 3. Real part of the ac magnetic susceptibility χ'_{ac} for Ba_2YWO_6 as a function of temperature at (a) different frequencies and (b) various dc magnetic fields. (c) Arrhenius plot for the activated frequency dependence of T_f. The blue solid line represents the Arrhenius fit to the data.

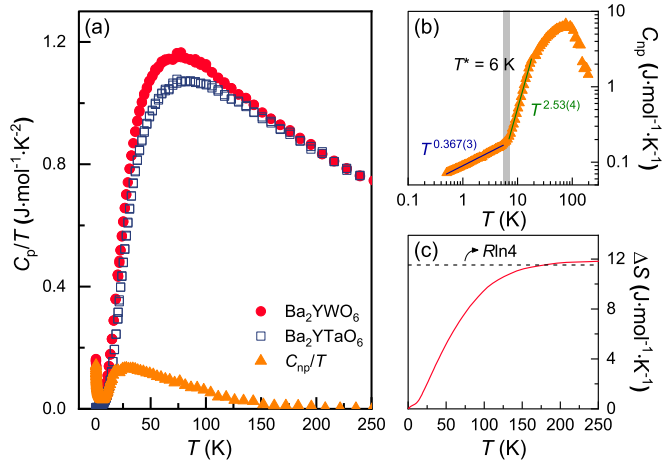

FIG. 4. (a) Temperature dependence of the specific heat divided by temperature C_p/T for Ba_2YWO_6 (circles) and its nonmagnetic counterpart Ba_2YTaO_6 (squares) under zero field. The triangle symbols represent the nonphononic contribution C_{np}/T. (b) Nonphononic specific heat as a function of temperature in a log-log scale. The colored solid lines denote the fits to the power-law behavior. (c) Temperature dependence of the spin-orbital entropy obtained by integrating C_{np}/T.

degenerate $j_{eff} = 3/2$ quartet. However, below 150 K, the Curie-Weiss fit provides $\Theta_{CW} = -7.8(1)$ K, $C = 0.02538(4)$ emu mol^{-1} K^{-1} Oe^{-1}, and $\mu_{eff} = 0.4505\ \mu_B$. The low-$T$ Curie constant indicates a 6.765% fraction of the $S = 1/2$ moments (or ~3.04% when the W^{5+} ions have $j_{eff} = 3/2$ where $g_J = 4/3$), which is comparable to the isostructural $4d^1$ DP Ba_2YMoO_6 [7,8]. Furthermore, the presence of the low-T linear regime in $1/\chi_{dc}(T)$ resembles that of Ba_2YMoO_6. However, the positive Θ_{CW} of Ba_2YWO_6 for high temperatures is in sharp contrast to the negative value of Ba_2YMoO_6 [7,8]. The T-varying Curie-Weiss parameters imply that the magnetic moments alone is insufficient to account for a magnetic behavior.

In the temperature range between $T = 3$–100 K, $\chi_{dc}(T)$ displays a non-Curie-Weiss increase. $\chi_{dc}(T)$ follows a power law $\chi_{dc}(T) \sim T^{-n}$ with $n = 0.75(1)$. The sub-Curie-Weiss behavior is regarded as a hallmark of random magnetism. For the random magnetism, the exponent emulates a distribution of exchange coupling constants. However, there is no clear evidence of chemical disorders in this system. As such, other mechanisms should be evoked to explain the T varying magnetic exchange interactions or magnetic moment along with the sub-Curie-Weiss behavior. Noteworthy is that a recent theoretical study proposed the mechanism for the strong temperature dependence of the effective magnetic moment for the d^1 DPs [5]. To be specific, for Ba_2YMoO_6, the pseudo-Jahn-Teller coupling enhances the mixing between the ground state and the excited spin-orbit multiplet states, giving rise to the reduction of the effective magnetic moment with decreasing temperature. In principle, a thermal variation of the pseudo-Jahn-Teller coupling can lead to an alteration of magnetic exchange interactions by modifying the orbital overlaps mediating exchange paths. Unlike Ba_2YMoO_6, however, the effective magnetic moments of Ba_2YWO_6 are enhanced at low temperatures. Thus, a future investigation is called for to ascertain whether a similar mechanism holds for Ba_2YWO_6.

The temperature dependence of the ac magnetic susceptibility $\chi'_{ac}(T)$ in various frequencies and magnetic fields are presented in Figs. 3(a) and 3(b). As the temperature is lowered, the broad maximum appears at $T_f \sim 0.3$ K. The observed cusp at T_f shifts to higher temperatures with increasing the frequency, while this is quickly suppressed by the application of the magnetic field. The frequency and field dependencies of $\chi'_{ac}(T)$ suggest the glassy nature of spin dynamics at low T. To estimate the activation energy, we plot the frequency dependence of $1/T_f$ in a semilog plot as shown in Fig. 3(c). $T_f(T, \nu)$ is well described with $\nu = \nu(0)\exp[-\Delta/k_B T_f]$, yielding the activation energy of $\Delta/k_B = 27.6$ K. The evaluated activation energy is comparable to that of Ba_2YMoO_6 ($\Delta/k_B = 39(2)$ K) [10].

B. Specific heat

Figure 4 shows the specific heat of Ba_2YWO_6, conveying information about low-energy excitations. To obtain the nonphononic specific heat $C_{np}(T)$, we subtract the lattice contribution from the total specific heat using the nonmagnetic counterpart Ba_2YTaO_6. Since both the compounds have similar molar mass, the phonon contribution to the specific heat is expected to be nearly identical. As displayed in Fig. 4(a), $C_p(T)/T$ of Ba_2YWO_6 matches well with that of Ba_2YTaO_6 above 175 K. Therefore, $C_{np}(T)$ should be ascribed to the singly occupied $5d\ t_{2g}$ level. With decreasing temperature, $C_{np}(T)/T$ exhibits a broad maximum at around 25 K and an upturn below 6 K. The broad maximum temperature is comparable with the estimated activation energy $\Delta/k_B = 27.6$ K from $\chi'_{ac}(T, \nu)$, suggesting the onset of partial moment

freezing. The low-T increment of $C_{\rm np}(T)/T$ cannot be reproduced by T^{-3}, thus, we rule out the possibility for nuclear Schottky contributions. Rather, the low-T upturning feature should be related to the density of low-energy magnetic excitations.

To determine the nature of low-lying excitations, we plot the temperature dependence of the nonphononic specific heat in a log-log scale as exhibited in Fig. 4(b). As the temperature is lowered, $C_{\rm np}(T)$ exhibits a broad hump at 75 K, which concurs with the power-law increment of $\chi_{\rm dc}(T)$. This implies the gradual spin-orbital freezing by quenching a degree of freedom for the orbitally degenerate $5d$ t_{2g} electrons. Upon cooling toward 0.3 K, $C_{\rm np}(T)$ exhibits two consecutive power-law behaviors T^n in the respective temperature range. The exponent changes from $n = 2.53(4)$ to 0.367(3) through $T^* = 6$ K. Notably, the power-law dependence of $C_{\rm np}(T) \sim T^{2.53(4)}$ is reminiscent of a spin-orbital liquid state, in which both spin and orbital are strongly correlated without long-range magnetic order [21–23]. However, Ba_2YWO_6 manifests the spin freezing at $T_{\rm f}$, as evident from the broad hump of $\chi'_{\rm ac}(T)$. Therefore, we infer that thermally activated $5d$ orbital fluctuations may give rise to the disordered spin-orbital liquid state in the intermediate temperature range $T = 6$–18 K. With decreasing temperature, the orbital fluctuations persist but diminish with the gradual moment freezing down to T^*. However, the weak power-law behavior below T^* suggests a small density of magnetic states at low energies. This can be interpreted as that while a majority of the magnetic moments are nullified by forming random singlets, a small fraction of the spins behave as free spins, supported by the activation behavior with $\Delta/k_{\rm B} = 27.6$ K.

The temperature dependence of the spin-orbital entropy $\Delta S(T)$ is shown in Fig. 4(c), which was calculated by integrating $C_{\rm np}(T)/T$. $\Delta S(T)$ shows the saturation to 11.82 J mol^{-1} K^{-1}, close to the $R\ln 4 = 11.52$ expected for a $j_{\rm eff} = 3/2$ quadruplet. As the $j_{\rm eff} = 1/2$ doublet lies at much higher energy, a single electron on $5d$ t_{2g} orbital should occupy the low-lying $j_{\rm eff} = 3/2$ quadruplet [24,25]. Given the small magnetic moment of $\sim$0.45 $\mu_{\rm B}$, a majority of the ΔS is of electronic origin. In the whole measured temperature range, we observe no discernible anomaly, ruling out the occurrence of apparent phase transitions. As such, our compound has no hint of an electric-quadrupolar ordering. With decreasing the temperature below T^*, only 2.4% of ΔS is released, in agreement with the $\sim$3.04% of the W^{5+} having $j_{\rm eff} = 3/2$ obtained from the Curie-Weiss fit to the low-T $\chi_{\rm dc}(T)$.

C. Muon spin relaxation

To rule out the possibility of long-range magnetic ordering, we carried out the weak transverse field (wTF) μSR experiments at various temperatures as shown in Fig. 5. In the wTF measurements, the long-range ordering would generally give rise to a loss of initial asymmetry ($t = 0$) or a rapidly relaxing component without muon precession signal due to the strongly developed static local fields, prevailing over the applied wTF. However, we observe no loss of initial asymmetry down to 26 mK and no rapidly damping component in the wTF-μSR data. Therefore, we rule out the establishment of local magnetic fields by the long-range ordering.

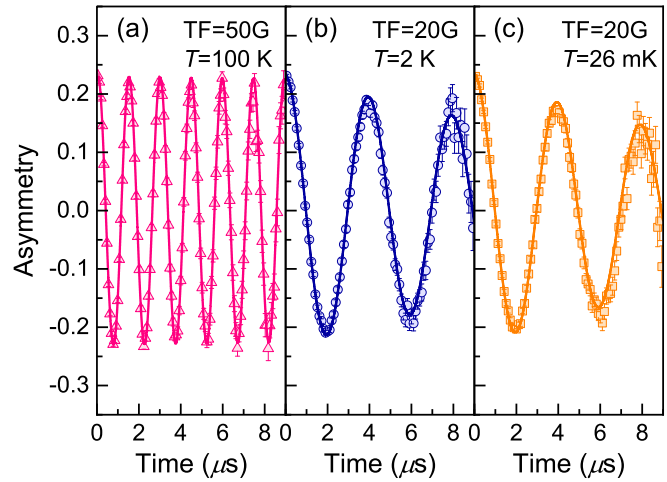

FIG. 5. Raw wTF-μSR spectra of Ba_2YWO_6 measured at (a) $T = 100$ K and $H_{\rm TF} = 50$ G, (b) $T = 2$ K and $H_{\rm TF} = 20$ G, and (c) $T = 26$ mK and $H_{\rm TF} = 20$ G, respectively. The solid curves represent the fits to the data.

The observed wTF data are well reproduced by a cosine function multiplied by a simple exponential function, $A_z(t) = A(0)\cos(2\pi f_\mu t + \phi)\exp(-\lambda_{\rm TF} t)$. Here, $A(0)$ is the initial asymmetry, f_μ is the muon Larmor precession frequency corresponding to the applied wTF, ϕ is the initial phase of the oscillatory signal, and $\lambda_{\rm TF}$ is the muon spin relaxation rate. With decreasing temperature, the muon spin relaxation increases and seems to saturate below 2 K.

We note that the raw wTF data show the initial asymmetry value of $\sim$0.27, suggesting that the observed slow relaxation in our μSR results is not a 1/3 tail of the muon depolarization but the total muon spin relaxation in the time window of continuous muon beam (see below). Hereafter, we plot the μSR data as polarization versus time after subtracting the time-independent background contribution (2–5% of the total asymmetry depending on the spectrometers). By this means, we match the initial muon spin polarization obtained from two different spectrometers.

We performed zero-field (ZF) and longitudinal-field (LF) μSR measurements to investigate the thermal and field evolution of spin-spin correlations. Figure 6(a) displays the ZF-μSR results of Ba_2YWO_6. We detect no evidence of the muon spin relaxation caused by nuclear depolarization, which suggests most muons stop near the O^{2-} ions. In the paramagnetic state, the muon spin depolarization is considerably slow, indicating the dominant muon spin relaxation by fast fluctuating moments at high temperatures. Furthermore, the ZF-μSR spectra show no signatures of static magnetism down to 26 mK, such as a coherent muon oscillating signal and 1/3 recovery of the muon polarization at long times. This seems to be at odds with the spin freezing at $T_{\rm f} \sim 0.3$ K, which will be discussed below.

For a quantitative analysis, the obtained ZF- and LF-μSR spectra of Ba_2YWO_6 are fitted with a single exponential function, $P_z(t) = P_z(0)\exp[-\lambda t]$. Here, $P_z(0)$ is the initial muon spin polarization at $t = 0$ and λ is the muon spin relaxation rate. The temperature dependence of the muon spin relaxation rate $\lambda(T)$ is shown in the inset of Fig. 6(a). As the

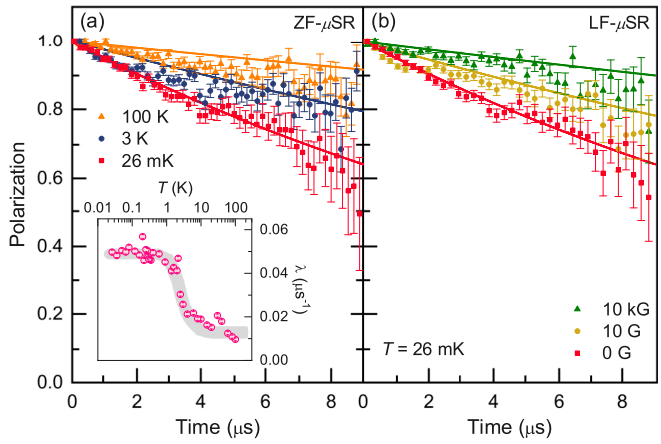

FIG. 6. (a) Representative ZF-μSR spectra at selected temperatures. The solid curves represent the fits to the data. The inset shows the temperature dependence of the muon spin relaxation rate $\lambda(T)$ on a semi-log scale. The shaded region is a guide to the eye. (b) LF dependence of μSR spectra measured at $T = 26$ mK.

temperature decreases, $\lambda(T)$ increases slightly and then exhibits the steep increase below 6 K. This suggests the slowing down of spin fluctuations by the development of spin correlations. Upon further cooling toward 26 mK, $\lambda(T)$ flattens out below 1 K, which signifies the entrance into the regime of persistent spin dynamics. Such a leveling-off behavior of the muon spin relaxation is observed in a range of frustrated magnets, including quantum spin liquid, spin freezing, spin glass, and weak magnetic order [26–28]. The persistent spin dynamics has been regarded as an indication of low-lying unconventional magnetic excitations whose origin is still under debate [28,29]. Therefore, the temperature-independent behavior of $\lambda(T)$ at low T suggests the presence of unconventional spin excitations in the $j_{\rm eff} = 3/2$ FCC Ba_2YWO_6.

To diagnose the dynamic nature of the ground state, we further carried out the LF-μSR experiments at 26 mK as shown in Fig. 6(b). The muon spin depolarization is recovered substantially by the applied weak LF of 10 G, approximately 15% at long times. This points to extremely weak fields generated by short-range correlations between the W spins at the muon interstitial sites. On further increasing the LF, the μSR spectra are nearly saturated, yet they still show the slow relaxation even in 10 kG. The persisting muon spin depolarization under 10 kG reflects the absence of static field distribution at the muon sites and the presence of dynamically fluctuating weak local fields in the ground state.

When the system has a conventional spin glass ground state, the μSR spectra are expected to be described by a Lorentzian Kubo-Toyabe-type function as in Sr_2MgReO_6 [30]. Otherwise, the μSR spectra can be generically fitted with the combined relaxation functions with the stretched exponential term $\exp[-(\lambda t)^{\beta}]$ and then the stretching exponent β is close to 1/3 below the spin freezing temperature [31–33]. However, neither case can be applied to our data within the time window of continuous muon beams, in which a simple exponential function well describes the μSR spectra. Instead, considering the low-T magnetic contributions to the magnetic and thermodynamic properties, the implanted muons relax predominantly by nearly freely propagating spins or spin singlets.

IV. DISCUSSION AND CONCLUSION

We discuss the ground state of Ba_2YWO_6. The dc and ac magnetic susceptibility measurements suggest the gradual formation of gapped singlets with decreasing temperature and subsequent spin freezing below $T_{\rm f} \sim 0.3$ K. However, the spin freezing is largely hidden to the μSR and specific heat data showing the absence of static magnetism down to 26 mK. Taken together, the ground state is approximated as randomly distributed spin-orbit dimers with dynamically fluctuating spin moments, a so-called valence-bond glass. We stress that the essentially same state is observed in the isostructural DP Ba_2YMoO_6 [7,8,10]. The valence-bond glass is expected to show the broad maximum in $C_{\rm np}(T)/T$, which is related to the energy scale of a spin-singlet formation [15]. As the temperature is lowered, the pseudogap is closed by the energy levels of emergent weakly coupled residual spins, evidenced by the gradual decrease of $C_{\rm np}(T)/T$ below 25 K. $C_{\rm np}(T)$ does not become zero down to 0.4 K, indicating the nonzero density of low-lying magnetic states. Furthermore, the power-law behavior of $\chi_{\rm dc}(T) \sim T^{-n}$ with $n = 0.75(1)$ is smaller than the theoretically predicted exponent $n = 1$ [15], yet it is compatible with random singlets [16]. As such, we expect a distribution of valence bonds in their size and strength. The observed magnetic and thermodynamic properties support the valence-bond glass state in Ba_2YWO_6.

A recent theoretical investigation has revealed that the magnetic phases in the d^1 cubic DPs can be tuned by the interplay of Hund's coupling and spin-orbit coupling [4]. Depending on both parameters, the magnetic phases are classified into a noncollinear antiferromagnetic or ferromagnetic phase, and a spin-orbit dimer phase. Despite the enhanced spin-orbit coupling by chemical substitution, Ba_2YWO_6 retains the valence-bond glass state. This observation is consistent with the existence of a wide spin-orbital dimer regime in the phase diagram [4]. Therefore, we purport that the valence-bond glass is stable toward the enhanced spin-orbit coupling as well as the isovalent chemical substitution of the A site [17].

We turn to the uncompensated weak magnetic moments, which govern the low-T magnetism. As evidenced by the activation behavior of $\chi'_{\rm ac}(T, \nu)$, most spins form the singlet state. Meanwhile, the orphanlike spins remain dynamically fluctuating, supported by the slow muon spin relaxation down at 26 mK. In addition, the negative $\Theta_{\rm CW} = -7.8(1)$ K below 150 K suggests weak exchange interactions between them at low temperatures. The orphanlike spins are nontrivial entities, which propagate through rearrangements of singlets. Based on these observations, we infer that the suppressed spin moments by orbital fluctuations are randomly distributed over the W sites with weak antiferromagnetic coupling at a longer distance. The occurrence of disparate magnetism can be understood in terms of time scales. At the macroscopic level, the majority of the spins gradually form the random spin-orbit singlets with decreasing temperature on the slow time scale, which is detectable in the bulk magnetic susceptibility. However, on the microscopic scale, the spins are subject to

quantum fluctuations. Such quantum fluctuations are incompetent for stabilizing the system into thermodynamically or quantum-mechanically ordered state [34–36], but this can be achieved at microscopic (fast) timescale (∼ns) [37].

In summary, our observations provide experimental evidence of a valence-bond glass in the $5d^1$ DP Ba_2YWO_6. The low-T Curie-Weiss regime in $\chi_{dc}(T)$ suggests that tiny fractions of spins contribute to the low-T magnetism, in agreement with a valence-bond glass at low temperatures. The pseudogap behavior and the subsequent change of the power-law exponent in $C_{np}(T)$ indicate a gradual formation of a valence bond glass with considerable orbital fluctuations. The μSR experiments determine that the quenched spin moments are weakly correlated in the background of the singlet states. Our results showcase that the $4/5d^1$ double perovskites are apt to host a valence bond glass, which can be regarded as a random version of the spin-orbit dimer state predicted in a three-dimensional FCC lattice.

ACKNOWLEDGMENTS

We thank B. Hitti and H. Luetkens for the technical support with μSR experiments in TRIUMF and PSI. The work at CAU was supported by the National Research Foundation (NRF) of Korea (Grants No. 2020R1A2C3012367 and No. 2020R1A5A1016518). G.W. and J.M. thank the financial support from the National Science Foundation of China (Grants No. 11774223 and No. U2032213). H.D.Z. acknowledges support from Brant No. NSF-DMR-2003117. A portion of this work was performed at the NHMFL, which is supported by National Science Foundation Cooperative Agreement No. DMR-1157490 and the State of Florida.

[1] W. Witczak-Krempa, G. Chen, Y. B. Kim, and L. Balents, Annu. Rev. Condens. Matter Phys. **5**, 57 (2014).
[2] S. Vasala and M. Karppinen, Prog. Solid State Chem. **43**, 1 (2015).
[3] G. Chen, R. Pereira, and L. Balents, Phys. Rev. B **82**, 174440 (2010).
[4] J. Romhányi, L. Balents, and G. Jackeli, Phys. Rev. Lett. **118**, 217202 (2017).
[5] N. Iwahara, V. Vieru, and L. F. Chibotaru, Phys. Rev. B **98**, 075138 (2018).
[6] E. J. Cussen, D. R. Lynham, and J. Rogers, Chem. Mater. **18**, 2855 (2006).
[7] M. A. de Vries, A. C. Mclaughlin, and J. W. G. Bos, Phys. Rev. Lett. **104**, 177202 (2010).
[8] T. Aharen, J. E. Greedan, C. A. Bridges, A. A. Aczel, J. Rodriguez, G. MacDougall, G. M. Luke, T. Imai, V. K. Michaelis, S. Kroeker, H. Zhou, C. R. Wiebe, and L. M. D. Cranswick, Phys. Rev. B **81**, 224409 (2010).
[9] J. P. Carlo, J. P. Clancy, T. Aharen, Z. Yamani, J. P. C. Ruff, J. J. Wagman, G. J. Van Gastel, H. M. L. Noad, G. E. Granroth, J. E. Greedan, H. A. Dabkowska, and B. D. Gaulin, Phys. Rev. B **84**, 100404(R) (2011).
[10] M. A. de Vries, J. O. Piatek, M. Misek, J. S. Lord, H. M. Rønnow, and J.-W. G. Bos, New J. Phys. **15**, 043024 (2013).
[11] K. G. Bramnik, H. Ehrenberg, J. K. Dehn, and H. Fuess, Solid State Sci. **5**, 235 (2003).
[12] C. A. Marjerrison, C. M. Thompson, G. Sala, D. D. Maharaj, E. Kermarrec, Y. Cai, A. M. Hallas, M. N. Wilson, T. J. S. Munsie, G. E. Granroth, R. Flacau, J. E. Greedan, B. D. Gaulin, and G. M. Luke, Inorg. Chem. **55**, 10701 (2016).
[13] K. E. Stitzer, M. D. Smith, and H.-C. zur Loye, Solid State Sci. **4**, 311 (2002).
[14] A. J. Steele, P. J. Baker, T. Lancaster, F. L. Pratt, I. Franke, S. Ghannadzadeh, P. A. Goddard, W. Hayes, D. Prabhakaran, and S. J. Blundell, Phys. Rev. B **84**, 144416 (2011).
[15] M. Tarzia and G. Biroli, Europhys. Lett. **82**, 67008 (2008).
[16] H. Kawamura and K. Uematsu, J. Phys.: Condens. Matter **31**, 504003 (2019).
[17] A. C. Mclaughlin, M. A. de Vries, and J. W. G. Bos, Phys. Rev. B **82**, 094424 (2010).
[18] K. Kiichiro, Y. Masahiro, N. Tetsuro, and S. Toshiyuki, Chem. Lett. **1**, 1201 (1972).
[19] Z. L. Dun, M. Lee, E. S. Choi, A. M. Hallas, C. R. Wiebe, J. S. Gardner, E. Arrighi, R. S. Freitas, A. M. Arevalo-Lopez, J. P. Attfield, H. D. Zhou, and J. G. Cheng, Phys. Rev. B **89**, 064401 (2014).
[20] A. Suter and B. M. Wojek, Phys. Procedia **30**, 69 (2012).
[21] Y. Kitaoka, T. Kobayashi, A. Kōda, H. Wakabayashi, Y. Niino, H. Yamakage, S. Taguchi, K. Amaya, K. Yamaura, M. Takano, A. Hirano, and R. Kanno, J. Phys. Soc. Jpn. **67**, 3703 (1998).
[22] V. Fritsch, J. Hemberger, N. Büttgen, E.-W. Scheidt, H.-A. Krug von Nidda, A. Loidl, and V. Tsurkan, Phys. Rev. Lett. **92**, 116401 (2004).
[23] Z. L. Dun, V. O. Garlea, C. Yu, Y. Ren, E. S. Choi, H. M. Zhang, S. Dong, and H. D. Zhou, Phys. Rev. B **89**, 235131 (2014).
[24] J. B. Goodenough, Phys. Rev. **171**, 466 (1968).
[25] A. S. Erickson, S. Misra, G. J. Miller, R. R. Gupta, Z. Schlesinger, W. A. Harrison, J. M. Kim, and I. R. Fisher, Phys. Rev. Lett. **99**, 016404 (2007).
[26] Y. Li, D. Adroja, P. K. Biswas, P. J. Baker, Q. Zhang, J. Liu, A. A. Tsirlin, P. Gegenwart, and Q. Zhang, Phys. Rev. Lett. **117**, 097201 (2016).
[27] P. Mendels, F. Bert, M. A. de Vries, A. Olariu, A. Harrison, F. Duc, J. C. Trombe, J. S. Lord, A. Amato, and C. Baines, Phys. Rev. Lett. **98**, 077204 (2007).
[28] A. Yaouanc, P. Dalmas de Reotier, A. Bertin, C. Marin, E. Lhotel, A. Amato, and C. Baines, Phys. Rev. B **91**, 104427 (2015).
[29] S. R. Dunsiger, R. F. Kiefl, K. H. Chow, B. D. Gaulin, M. J. P. Gingras, J. E. Greedan, A. Keren, K. Kojima, G. M. Luke, W. A. MacFarlane, N. P. Raju, J. E. Sonier, Y. J. Uemura, and W. D. Wu, Phys. Rev. B **54**, 9019 (1996).
[30] C. R. Wiebe, J. E. Greedan, P. P. Kyriakou, G. M. Luke, J. S. Gardner, A. Fukaya, I. M. Gat-Malureanu, P. L. Russo, A. T. Savici, and Y. J. Uemura, Phys. Rev. B **68**, 134410 (2003).
[31] Y. J. Uemura, T. Yamazaki, D. R. Harshman, M. Senba, and E. J. Ansaldo, Phys. Rev. B **31**, 546 (1985).
[32] I. A. Campbell, A. Amato, F. N. Gygax, D. Herlach, A. Schenck, R. Cywinski, and S. H. Kilcoyne, Phys. Rev. Lett. **72**, 1291 (1994).

[33] A. Keren, P. Mendels, I. A. Campbell, and J. Lord, Phys. Rev. Lett. **77**, 1386 (1996).
[34] C. Chamon, Phys. Rev. Lett. **94**, 040402 (2005).
[35] T. E. Markland, J. A. Morrone, B. J. Berne, K. Miyazaki, E. Rabani, and D. R. Reichman, Nat. Phys. **7**, 134 (2011).
[36] C. Castelnovo and C. Chamon, Philos. Mag. **92**, 304 (2012).
[37] O. G. Shpyrko, E. D. Isaacs, J. M. Logan, Y. Feng, G. Aeppli, R. Jaramillo, H. C. Kim, T. F. Rosenbaum, P. Zschack, M. Sprung, S. Narayanan, and A. R. Sandy, Nature (London) **447**, 68 (2007).